

Electronic Supplementary Information

Non-fullerene acceptors based on central naphthalene diimide flanked by rhodanine or 1,3-indanedione

Doli Srivani,^{a,b} Akhil Gupta,^{*c} Avinash L. Puyad,^d Wanchun Xiang,^e Jingliang Li,^c Richard A. Evans,^f Sheshanath V. Bhosale^{*g} and Sidhanath V. Bhosale^{*a}

a Polymers and Functional Materials Division, CSIR-Indian Institute of Chemical Technology, Hyderabad 500007 Telangana, India. bhosale@iict.res.in

b Academy Scientific and Innovative Research (AcSIR), CSIR-IICT, Hyderabad 500007, Telangana, India

c Institute for Frontier Materials, Deakin University, Waurn Ponds, Victoria 3216 Australia; Tel: +61 3 5247 9542; E-mail: akhil.gupta@deakin.edu.au; <http://orcid.org/0000-0002-1257-8104>

d School of Chemical Sciences, Swami Ramanand Teerth Marathwada University, Nanded 431606 Maharashtra, India

e State Key Laboratory of Silicate Materials for Architectures, Wuhan University of Technology, 122 Luoshi Rd, Wuhan 430070 Hubei, P. R. China

f CSIRO Manufacturing, Bayview Avenue, Clayton South, Victoria 3169 Australia

g School of Science, RMIT University, GPO Box 2476, Melbourne, Victoria 3001 Australia; E-mail: sheshanath.bhosale@rmit.edu.au

Table of contents

Experimental details.....	S3–S4
Synthetic details.....	S4–S6
Blend film spectra.....	S6
Detailed DFT calculations.....	S7–S13
Energy level diagram.....	S13
PESA curves.....	S14
CV data	S15–S16
TGA curves.....	S17
DSC curves.....	S18
Table S4 (Photovoltaic cell parameters)	S19
IPCE spectra.....	S19
XRD spectra.....	S20
SCLC Details.....	S20–S21
Experimental spectra.....	S22–S25
References.....	S26

Experimental details

Materials and methods

Materials: Rhodanine, 1,3-indandione and pyrrolidine were purchased from Sigma -Aldrich Co., Bengaluru, Karnataka, India. Piperidine was purchased from Avra Synthesis Pvt Ltd. Acetonitrile was purchased from S. D. Fine Chemicals Limited (SDFCL), India. Dichloromethane and methanol (both AR grade) were purchased from Finar chemicals, India and were used without further purification. Synthesis of 5,5'-(2,7-dioctyl-1,3,6,8-tetraoxo-1,2,3,6,7,8-hexahydrobenzo[*lmn*][3,8]phenanthroline-4,9-diyl)bis(thiophene-2-carbaldehyde) was reported previously.^{S1}

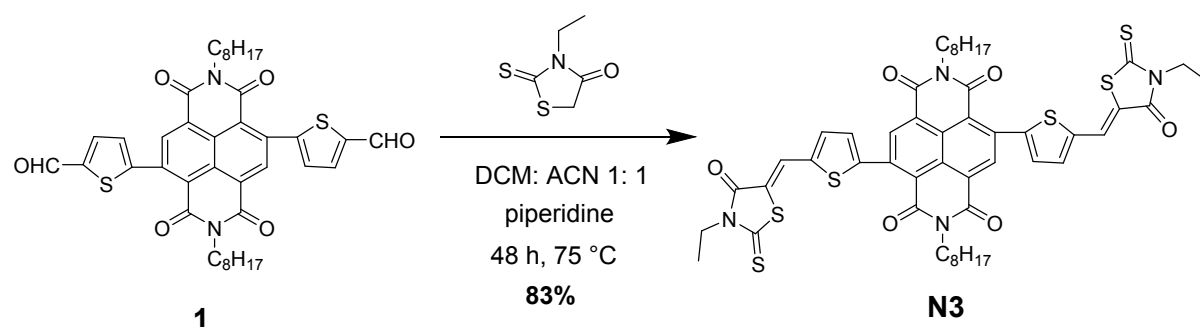
General details: All reactions were performed under an inert atmosphere of anhydrous nitrogen gas unless otherwise stated. Solvents used for various reactions were dried using a commercial solvent purification system. Solvents used in reaction extractions and chromatography, and all other reagents were used as supplied by commercial vendors without further purifications or drying. Thin layer chromatography (TLC) was performed using 0.25 mm thick plates pre-coated with silica gel (40–60 μm , F₂₅₄) and visualized using UV light (254 and 365 nm). Petroleum spirits with a boiling point range of 40–60 °C was used wherever indicated. Column chromatography was performed on either 40–60 or 20–40 μm silica gel. ¹H NMR spectra were recorded at 300, 400 or 500 MHz as indicated. The following abbreviations were used to explain multiplicities: s = singlet, d = doublet, t = triplet, q = quartet, m = multiplet, br = broad, dd = doublet of doublets, and dt = doublet of triplets. ¹³C NMR spectra were recorded at 75, 101 or 125 MHz as indicated. ¹H and ¹³C chemical shifts were calibrated using residual non-deuterated solvent as an internal reference and are reported in parts per million (δ) relative to tetramethylsilane ($\delta = 0$). IR-Spectra were recorded on Thermo Nicolet Nexus 670 spectrometer in the form of non-hygroscopic KBr pellets. MALDI spectra were taken from Shimadzu Biotech Axima Performance instrument. For high-resolution mass spectra (HRMS), atmospheric-pressure chemical ionization (APCI) experiments were carried out on FTMS, ionizing by APCI from an atmospheric solids analysis probe (ASAP). DSC experiments were carried out by using Q-100 DSC instrument with nitrogen as a purging gas. Samples were heated to 350 °C at a heating rate of 10 °C/minute. TGA experiments were carried out using Q-500 TGA instrument with nitrogen as a purging gas. Samples were heated to 800 °C at a rate of 10 °C/minute under nitrogen atmosphere. UV–Vis absorption spectra were recorded using a Hewlett Packard HP 8453 diode array spectrometer. PESA measurements were recorded

using a Riken Keiki AC-2 PESA spectrometer with a power setting of 5 nW and a power number of 0.5. Samples for PESA were prepared on cleaned glass substrates. Electrochemical measurements were carried out using a PowerLab ML160 potentiostat interfaced via a PowerLab 4/20 controller to a PC running E-Chem for Windows version 1.5.2. The measurements were run in argon-purged dichloromethane with tetrabutylammoniumhexafluorophosphate (0.1 M) as the supporting electrolyte. The cyclic voltammograms were recorded using a standard three electrode configuration with a glassy carbon (2 mm diameter) working electrode, a platinum wire counter electrode and a silver wire pseudo reference electrode. The silver wire was cleaned in concentrated nitric acid followed by concentrated hydrochloric acid and then washed with deionised water. Cyclic voltammograms were recorded with a sweep rate of 50 mV s⁻¹. All the potentials were referred to the E_{1/2} of ferrocene/ferrocenium redox couple.

Details of device fabrication and characterization of photovoltaic devices were reported previously.^{S2,S3} Atomic force microscopy (AFM) topographic maps were directly performed on the active layers of the P3HT: **N3/N4** blends using an Asylum Research MFP-3D-SA instrument. The AFM was run in intermittent contact mode (tapping mode) using MicroMasch NSC18 tips (typical resonant frequency ~100 kHz, typical probe radius ~10 nm and typical aspect ratio 3: 1). A Bruker AXS D8 Discover instrument with a general area detector diffraction system (GADDS) using Cu K α source was utilized to obtain XRD patterns.

Synthetic details

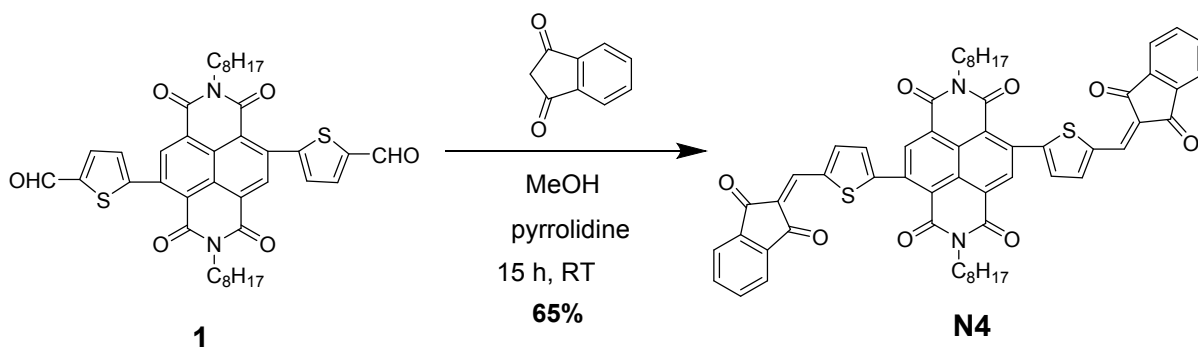
Synthesis of compound **N3**:



4,9-Bis(5-((Z)-(3-ethyl-4-oxo-2-thioxothiazolidin-5-ylidene)methyl)thiophen-2-yl)-2,7-dioctylbenzo[*lmn*][3,8]phenanthroline-1,3,6,8(2*H*,7*H*)-tetraone (N3**):** To a mixture of 5,5'-(2,7-dioctyl-1,3,6,8-tetraoxo-1,2,3,6,7,8-hexahydrobenzo[*lmn*][3,8]phenanthroline-4,9-diyl)bis(thiophene-2-carbaldehyde) (**1**) (120 mg, 0.169 mmol) and *N*-ethyl rhodanine (59.0 mg,

0.371 mmol) in 30.0 mL of dichloromethane: acetonitrile (1: 1) was added piperidine (84.0 μ L, 0.85 mmol), and the resultant reaction mixture was refluxed for 48 h at 75 $^{\circ}$ C. The completion of reaction was confirmed by TLC. The reaction mixture was cooled and poured into precooled water containing hydrochloric acid and was extracted with dichloromethane. The organic layer was dried over Na_2SO_4 , filtered and evaporated under reduced pressure. The crude product was purified by silica gel column chromatography using dichloromethane: hexane (6: 4, v/v) to afford title product (**N3**) as a cherry solid (130 mg, 83%). ^1H NMR(CDCl_3 , 400 MHz, ppm) δ 8.77–8.75 (s, 2H), 7.95–7.93 (s, 2H), 7.52–7.49 (d, $J = 4.2$ Hz, 2H), 7.38–7.35 (d, $J = 4.2$ Hz, 2H), 4.25–4.17 (q, 4H), 4.14–4.08 (t, 4H), 1.72–1.62 (m, 4H), 1.36–1.23 (m, 26H), 0.88–0.82 (t, 6H); ^{13}C NMR (CDCl_3 , 125 MHz) δ 191.78, 167.23, 161.70, 147.78, 140.31, 138.84, 136.05, 133.80, 130.01, 127.72, 125.74, 124.59, 123.65, 122.36, 41.35, 40.01, 31.75, 29.24, 29.16, 27.99, 27.03, 22.60, 14.06, 12.27; FT-IR (KBr, cm^{-1}) ν 3422, 2922, 2852, 1698, 1659, 1583, 1434, 1376, 1346, 1316, 1213, 1175, 1131, 1080, 1010, 878, 816, 792, 761, 736, 664, 551, 511; MALDI-TOF ($\text{M}+\text{H}^+$): 997.06; HRMS (APCI): Calculated for (M^+): $\text{C}_{50}\text{H}_{52}\text{N}_4\text{O}_6\text{S}_6 = 996.2206$; found = 996.2208.

Synthesis of compound **N4**:



4,9-Bis(5-((1,3-dioxo-1,3-dihydro-2H-inden-2-ylidene)methyl)thiophen-2-yl)-2,7-dioctylbenzo[*lmn*][3,8]phenanthroline-1,3,6,8(2H,7H)-tetraone (N4**):** To a mixture of compound **1** (250 mg, 0.35 mmol) and 1,3-indanedione (154 mg, 1.05 mmol) in 30.0 mL of dry methanol was added pyrrolidine (143 μ L, 1.75 mmol), and the resultant reaction mixture was stirred at room temperature for 15 h. The completion of reaction was confirmed by TLC. The reaction mixture was poured into precooled water containing hydrochloric acid and was extracted with dichloromethane. The organic layer was dried over Na_2SO_4 , filtered and evaporated under reduced pressure. The crude product was purified by silica gel column

chromatography using dichloromethane: hexane (7: 3, v/v) to afford title product (**N4**) as a brick red solid (221 mg, 65%). ^1H NMR (CDCl_3 , 400 MHz, ppm) δ 8.81–8.78 (s, 2H), 8.10–8.08 (d, 2H), 8.08–8.07 (s, 2H), 8.03–7.96 (m, 4H), 7.84–7.78(m, 4H), 7.39–7.37 (d, 2H), 4.14–4.06 (t, 4H), 1.72–1.60 (m, 4H), 1.41–1.17 (m, 20H), 0.92–0.80 (t, 6H); ^{13}C NMR ($\text{CDCl}_3/\text{deuterated TFA}$, 125 MHz ppm) δ 191.67, 162.91 155.20, 144.71, 141.28, 139.76, 139.38, 139.31, 136.83, 136.46, 136.37, 130.00, 127.86, 125.71, 124.26, 124.13, 123.86, 42.06, 31.73, 29.12, 27.84, 26.96, 22.56, 13.84; FT-IR (KBr, cm^{-1}) ν 3530, 2924, 2851, 1706, 1699, 1669, 1578, 1434, 1375, 1346, 1311, 1240, 1204, 1091, 1018, 990, 813, 795, 734, 665, 634, 538, 458; MALDI-TOF ($\text{M}+\text{H}$) $^+$ = 967.03; HRMS (APCI): Calculated for (M) $^+$: $\text{C}_{58}\text{H}_{50}\text{N}_2\text{O}_8\text{S}_2$ = 966.3003; found = 966.3000.

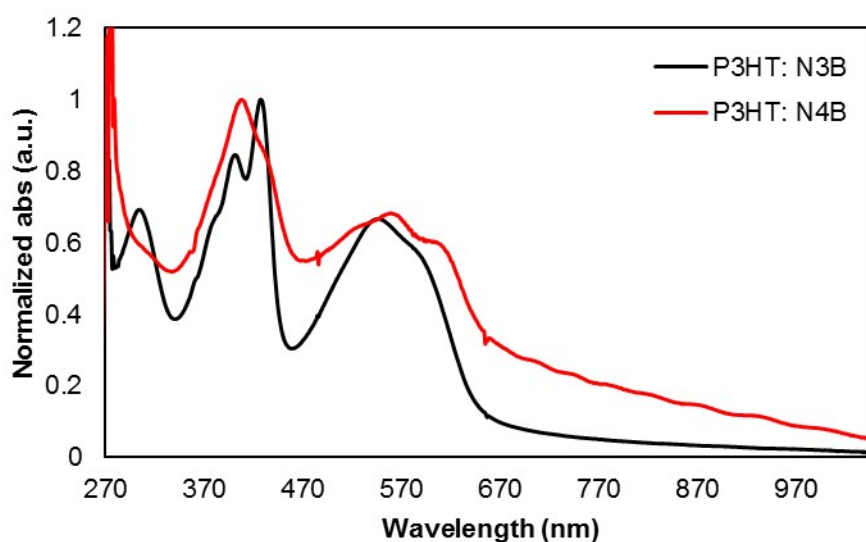


Fig. S1 Blend film absorption spectra of **N3** and **N4** with the defined weight ratio of 1: 1.2 donor: acceptor

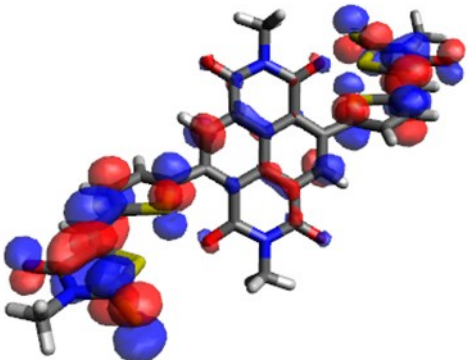
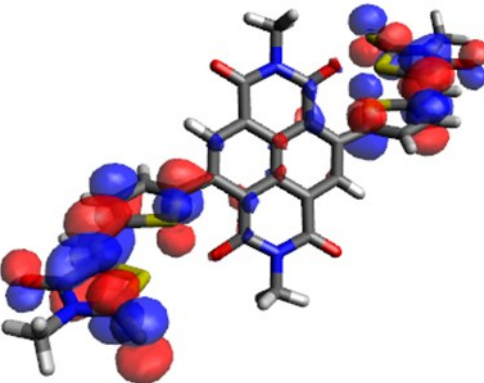
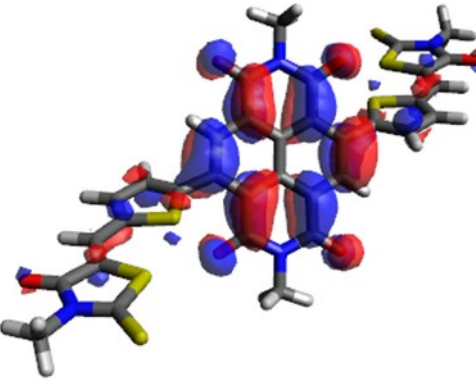
Detailed DFT calculations^{S4,S5,S6}

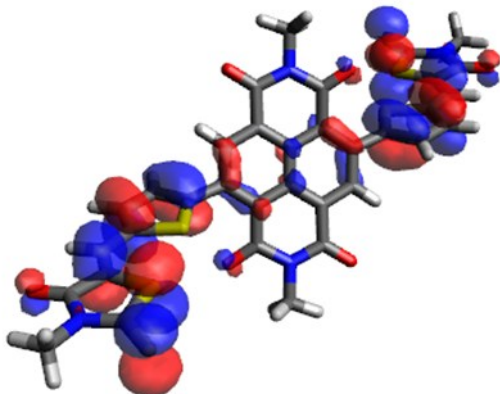
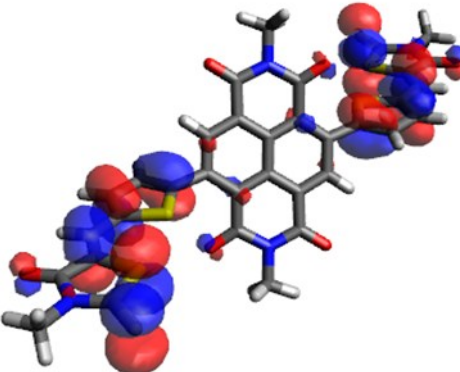
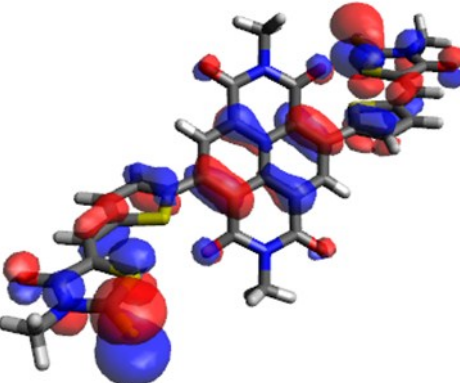
From the TD-DFT results it is seen that **N3** shows absorption peaks at 353 nm and 457 nm whereas **N4** shows absorption peaks at 344 nm and 432 nm, a finding corroborating our experimental analysis. The frontier molecular orbitals (FMOs) calculated at the CAM-B3LYP/6-31G(d) level of theory and generated using Avogadro are given below in Fig. S1.

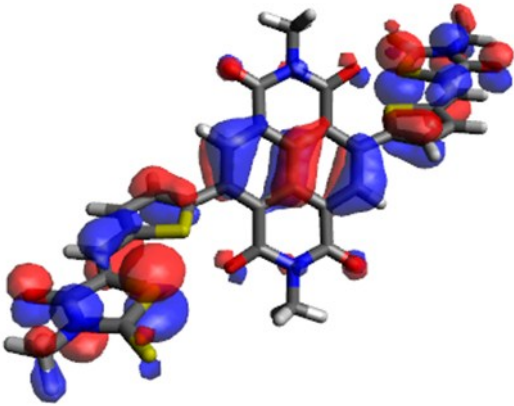
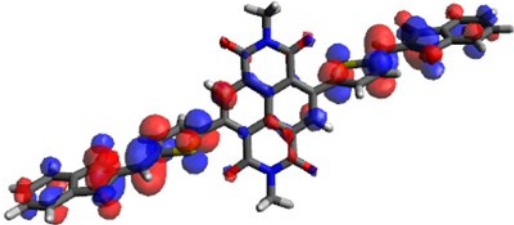
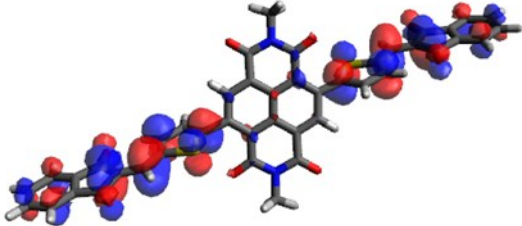
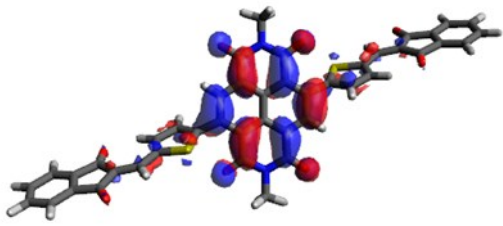
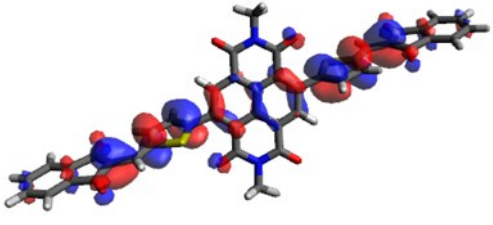
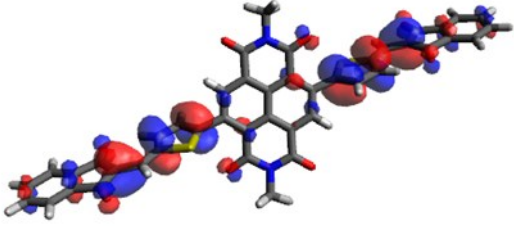
Table S1: Calculated TD-DFT excitation properties of **N3** and **N4**

Molecules	Excitation Energy(eV)	Excitation Wavelength(nm)	Oscillator Strength(f)	Excitations
N3	2.7141	457	0.8078	189 → 199 (H-9 → L)
				194 → 199 (H-4 → L)
				197 → 200 (H-1 → L+1)
				198 → 199 (H → L)
	3.5109	353	1.5527	194 → 199 (H-4 → L)
				197 → 200 (H-1 → L+1)
				198 → 199 (H → L)
				198 → 201 (H → L+2)
N4	2.8731	432	1.0253	185 → 199 (H-13 → L)
				197 → 200 (H-1 → L+1)
				198 → 199 (H → L)
				198 → 201 (H → L+2)
	3.6021	344	1.9673	194 → 199 (H-4 → L)
				197 → 200 (H-1 → L+1)
				198 → 199 (H → L)
				198 → 201 (H → L+2)

Frontier molecular orbitals of N3 and N4

N3-m		eV	
201	L+2	-1.6675	
200	L+1	-1.7225	
199	L	-2.7998	

198	H	-7.2677	
197	H-1	-7.3953	
194	H-4	-8.4361	

189	H-9	-9.0849	
N4-m			
201	L+2	-1.5829	
200	L+1	-1.6275	
199	L	-2.6784	
198	H	-7.4380	
197	H-1	-7.6021	

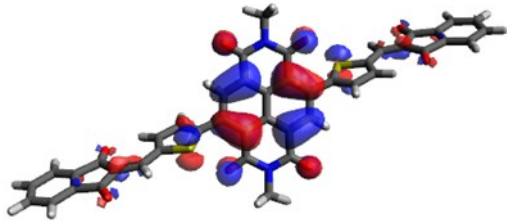
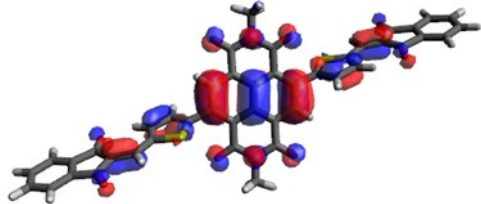
194	H-4	-8.5640	
185	H-13	-9.2294	

Fig. S2 Frontier molecular orbitals of **N3** and **N4** with energy levels in eV.

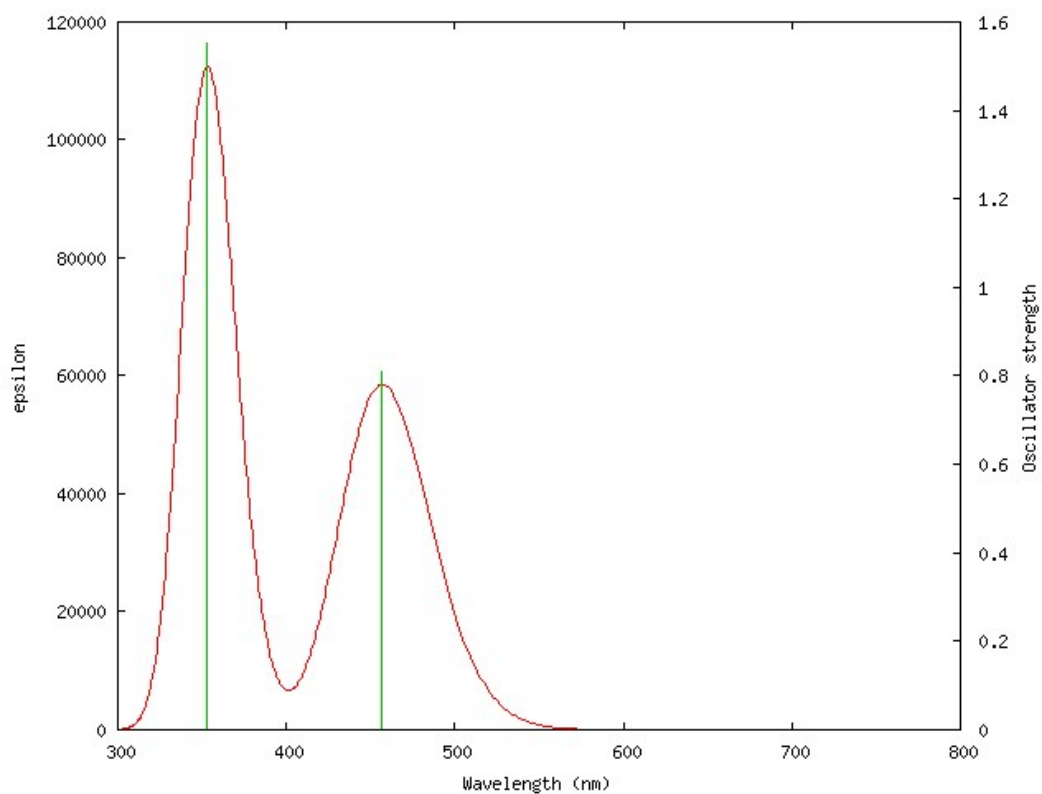


Fig. S3 Theoretical optical absorption spectrum of **N3**.

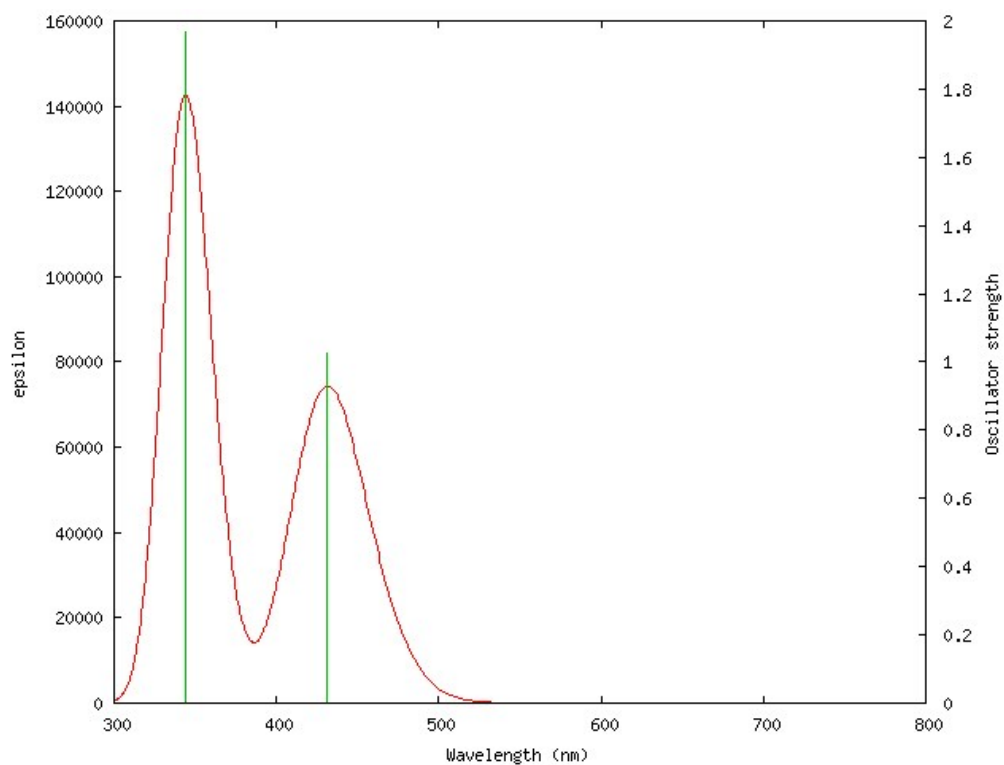


Fig. S4 Theoretical optical absorption spectrum of N4.

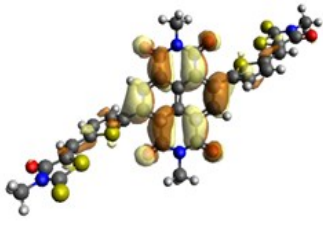
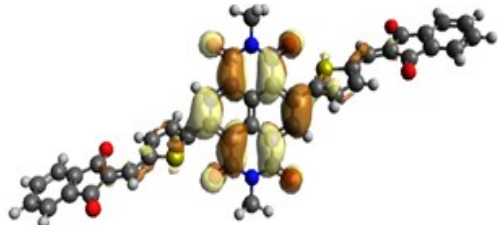
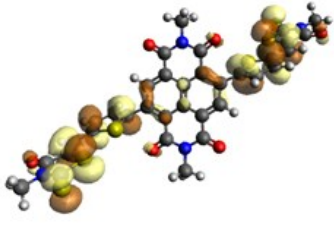
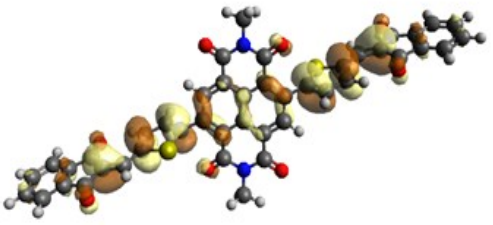
NTO nomenclature	N3	N4
Electron		
Hole		

Fig. S5 A pair of NTOs with a very similar character as the corresponding hole/electron pair

Table S2 Percentage contributions for transitions in **N3** and **N4**

Percentage contributions for transitions in N3 *			
Wavelength (nm)	Oscillator Strength	Major contributions	Minor contributions
457	0.8078	H → L (82%)	H-9 → L (3%), H-4 → L (5%), H-1 → L+1 (6%)
353	1.5527	H-1 → L+1 (35%), H → L+2 (49%)	H-4 → L (3%), H → L (3%)
Percentage contributions for transitions in N4 *			
Wavelength (nm)	Oscillator Strength	Major contributions	Minor contributions
432	1.0253	H → L (84%)	H-13 → L (2%), H-1 → L+1 (6%)
344	1.9673	H-4 → L (17%), H-1 → L+1 (31%), H → L+2 (41%)	H → L (3%)

*major contribution is from transition involving HOMO to LUMO

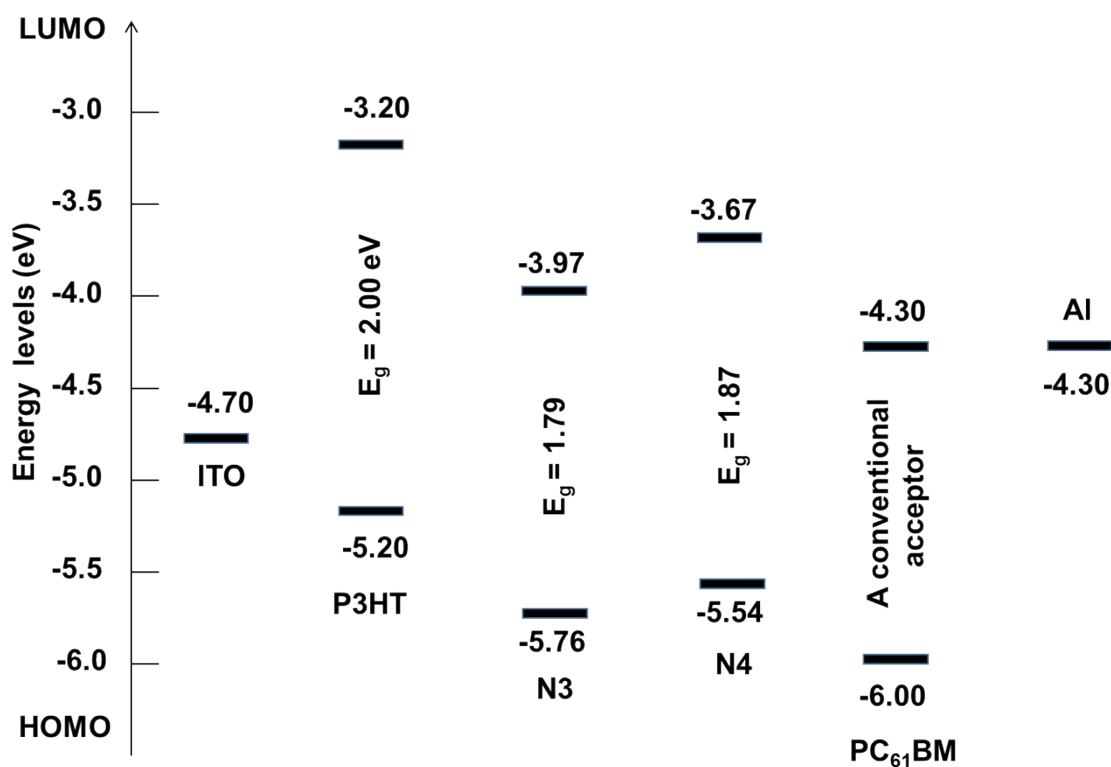


Fig. S6 Energy level diagram showing alignments of different components of a BHJ device architecture.

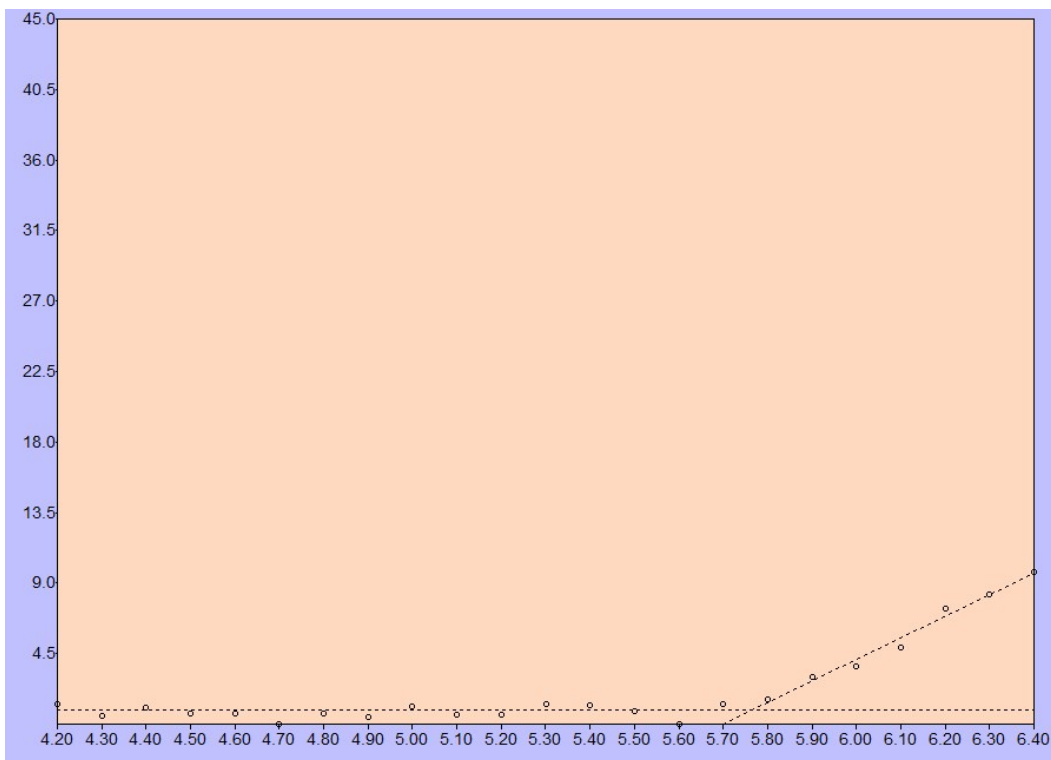


Fig. S7 PESA curve of N3.

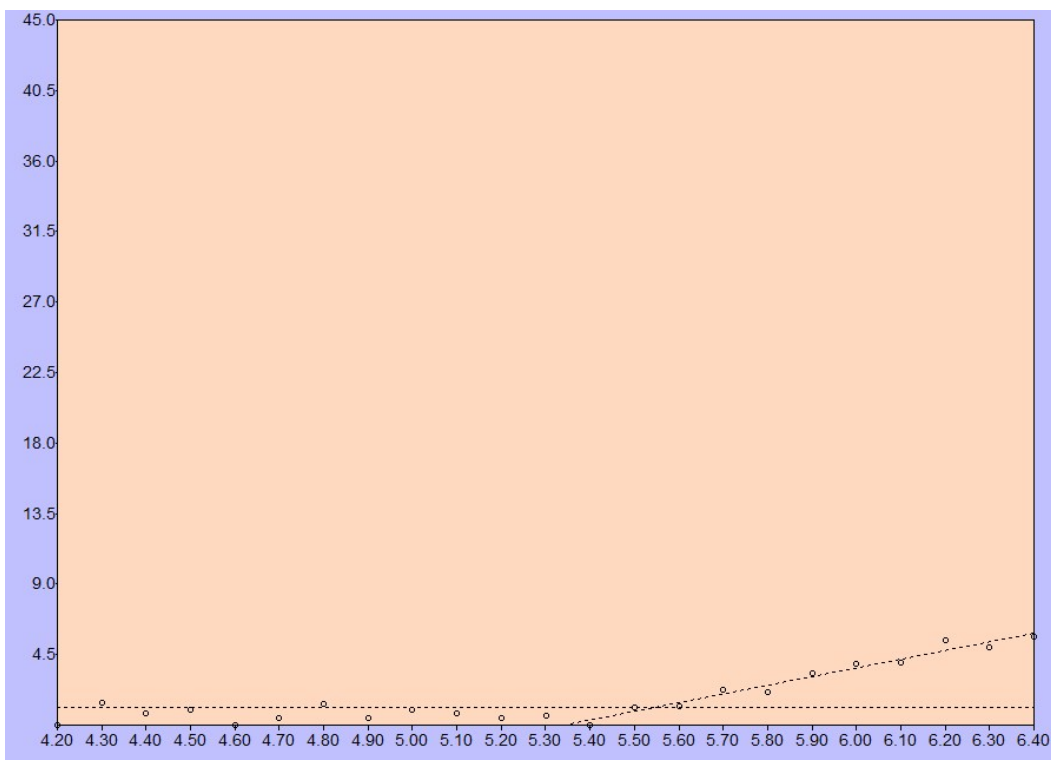


Fig. S8 PESA curve of N4.

Cyclic-voltammetry data:

Cyclic-voltammograms indicated that the reduction of **N3** and **N4** occurred at a half-wave potential of around 0.5 eV vs ferrocene/ferrocenium (F_c/F_c^+) internal reference, thus providing overall band-gaps of 1.97 eV and 2.16 eV (Table S3), respectively, a finding consistent with the PESA study.

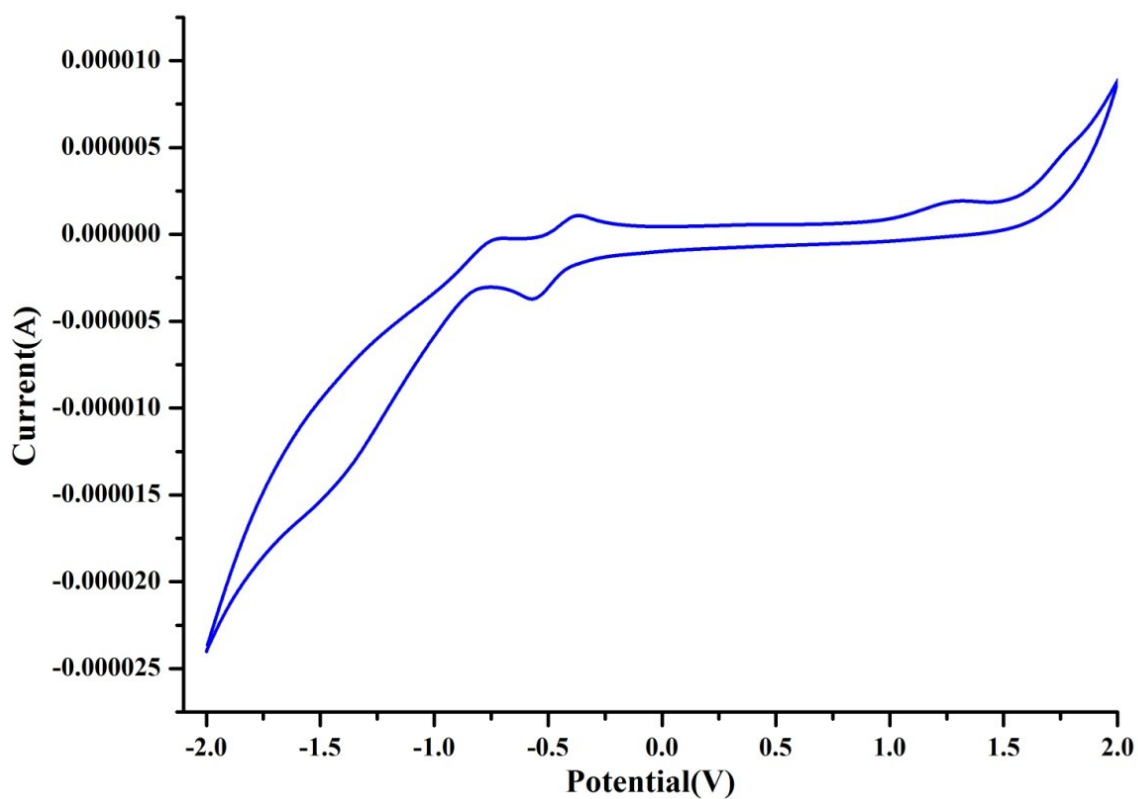


Fig. S9 Cyclic-voltammogram of **N3**.

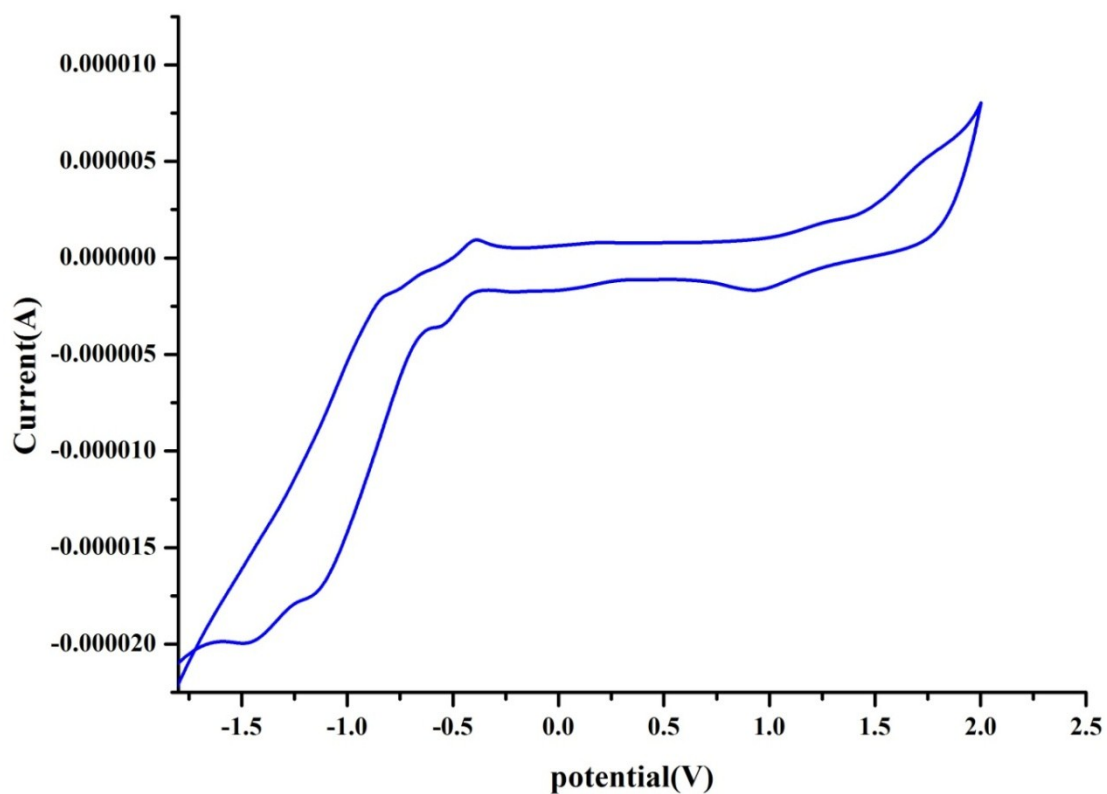


Fig. S10 Cyclic-voltammogram of **N4**

Table S3 Comparative electrochemical data obtained from CV

Sr. No.	Molecule	$E_{\text{red}}^{\text{onset}}$	$E_{\text{oxd}}^{\text{onset}}$	E_{LUMO}	E_{HOMO}	E_{gap}
1	N3	-0.497	-	-3.90 eV	-5.87 eV	1.97 eV
2	N4	-0.503	-	-3.89 eV	-6.05 eV	2.16 eV

Sample: SVB-SC4-P1
Size: 1.3920 mg
Method: Ramp

TGA

File: H:\SVB-SC4-P1.001

Run Date: 09-Sep-16 11:13
Instrument: TGA Q500 V20.13 Build 39

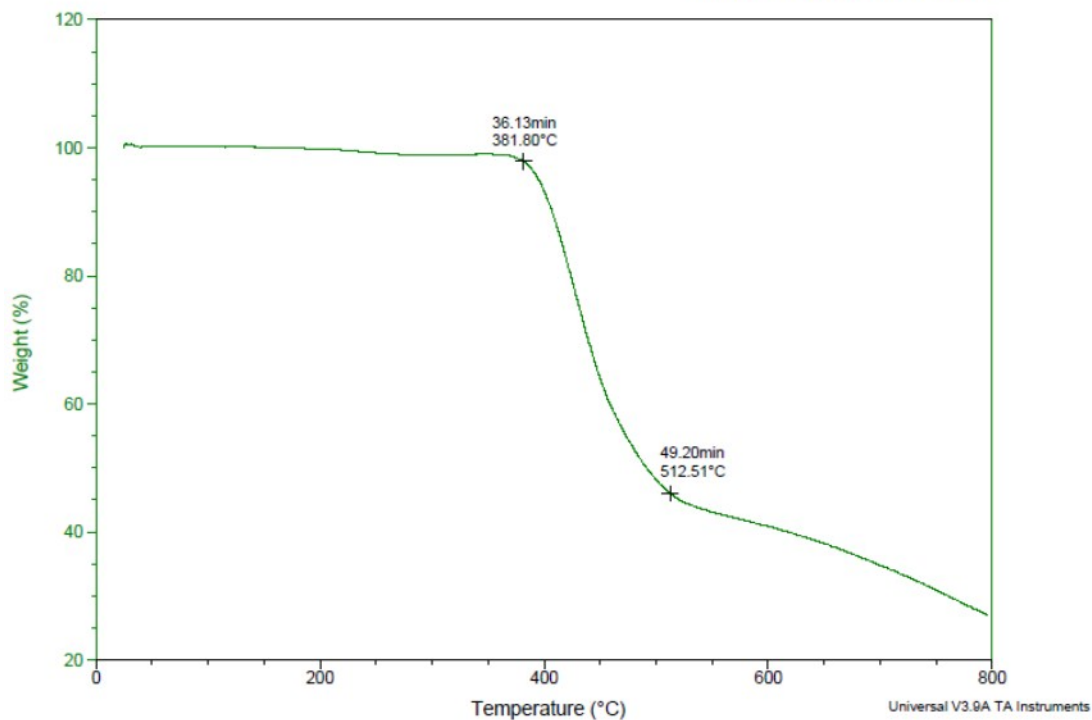


Fig. S11 TGA curve of N3 (heating up to 800 °C at the rate of 10 °C/minute).

Sample: SVB-SC4-P2
Size: 1.7640 mg
Method: Ramp

TGA

File: H:\SVB-SC4-P2.001

Run Date: 09-Sep-16 14:22
Instrument: TGA Q500 V20.13 Build 39

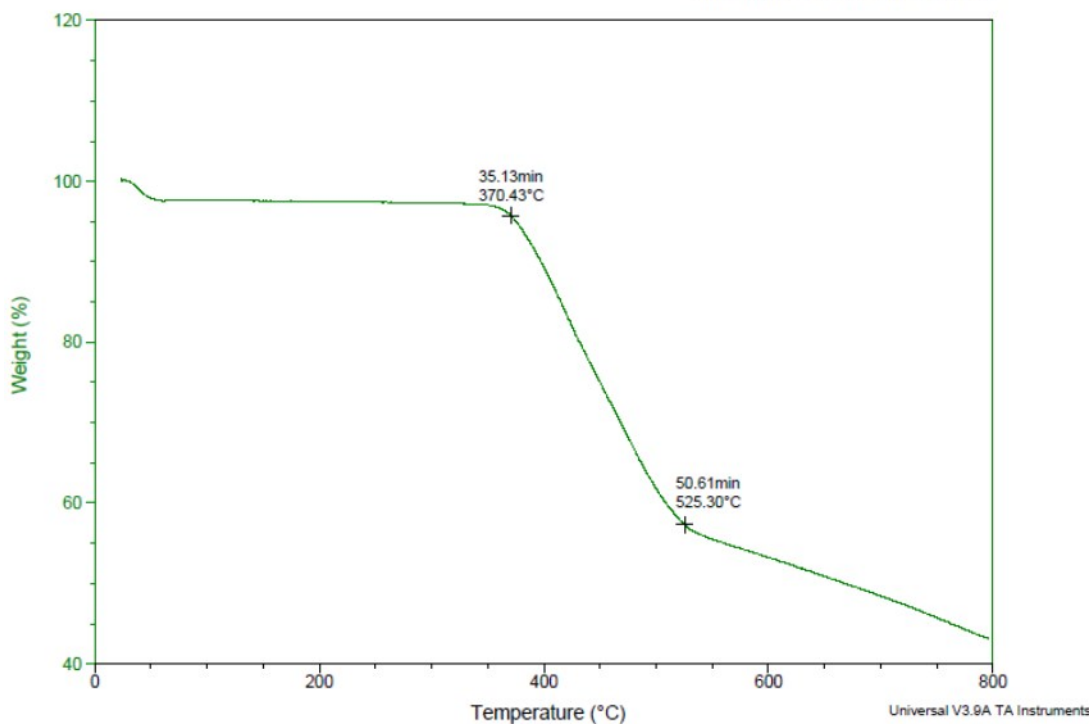


Fig. S12 TGA curve of N4 (heating up to 800 °C at the rate of 10 °C/minute).

Sample: SVB-S4-P1
Size: 1.8000 mg
Method: Ramp
Comment: SVB-S4-P1

DSC

File: H:\sec-Dsc\SVB-S4-P1.001
Operator: SANDEEP
Run Date: 22-Aug-16 14:58
Instrument: DSC Q100 V9.5 Build 288

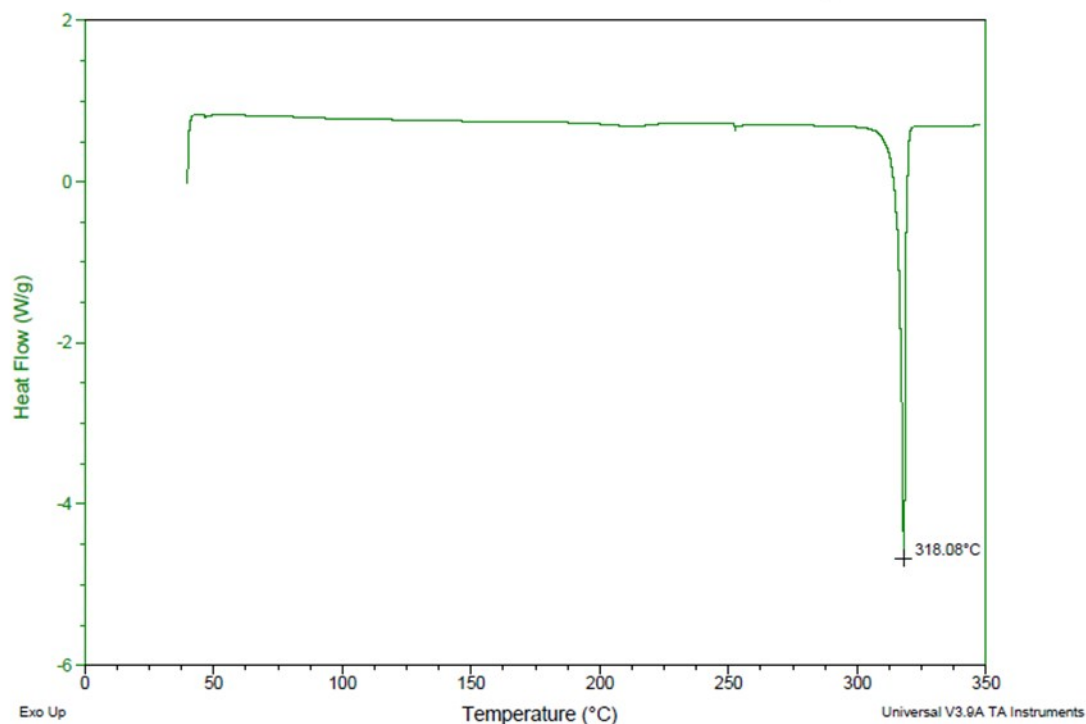


Fig. S13 DSC curve of N3 (heating up to 350 °C at the rate of 10 °C/minute).

Sample: NDI-N4
Size: 3.4000 mg

DSC

File: H:\NDI-N4.001
Operator: SANDEEP
Run Date: 24-Jan-17 14:55
Instrument: DSC Q100 V9.5 Build 288

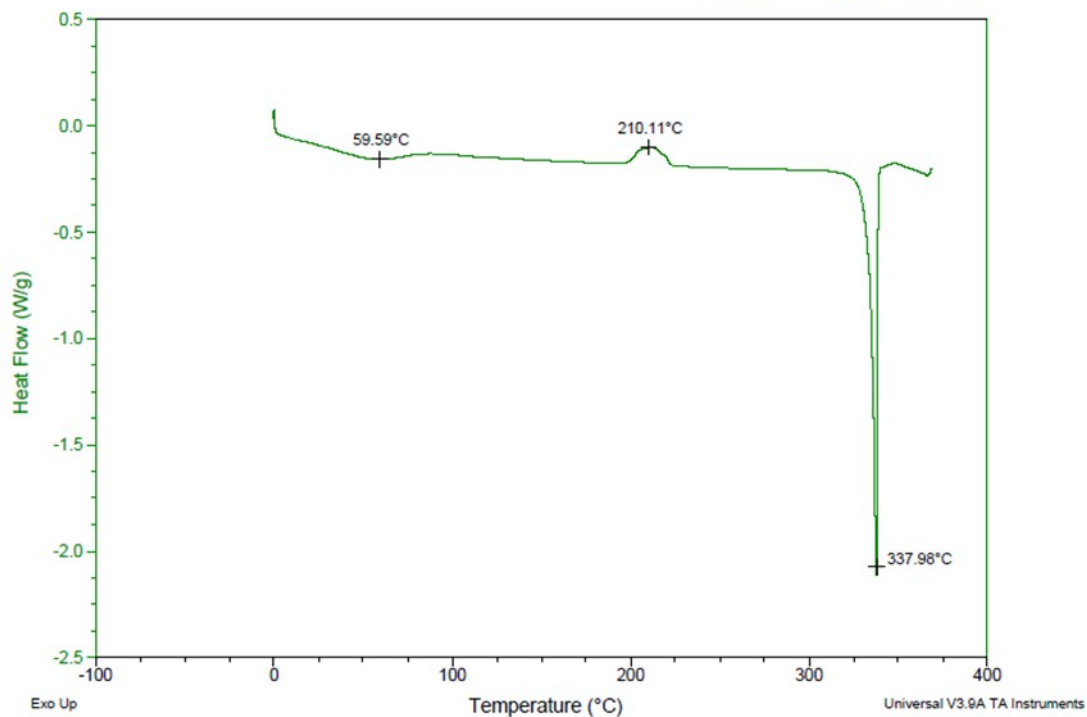


Fig. S14 DSC curve of N4 (heating up to 350 °C at the rate of 10 °C/minute).

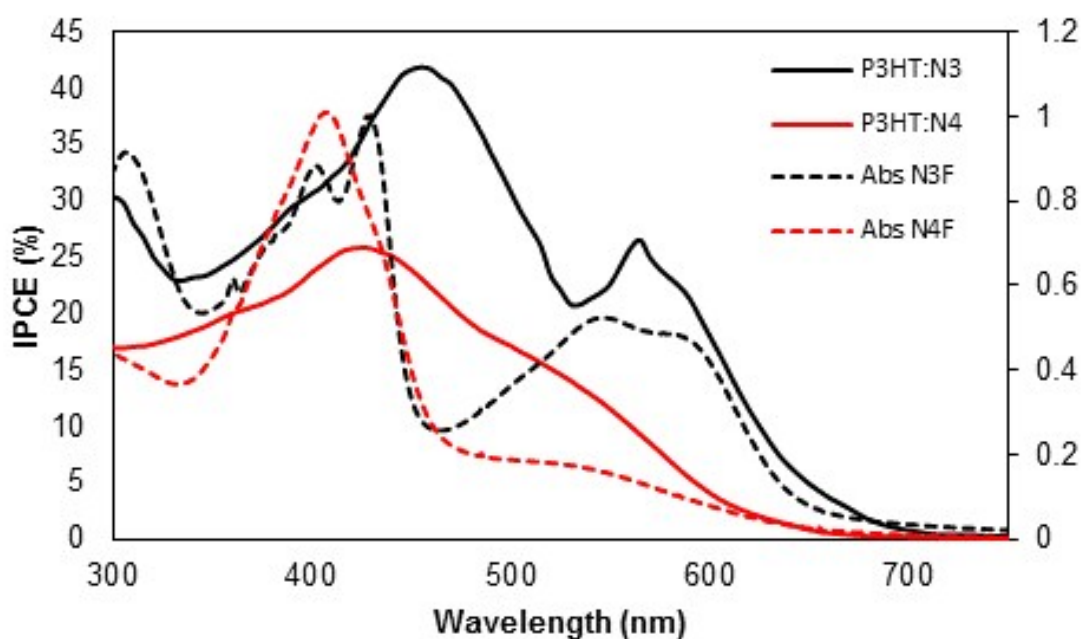
Table S4 Photovoltaic cell parameters for P3HT: N3/ N4 blends under different conditions

Material	Testing conditions (donor: acceptor) ^a	V_{oc} (V)	J_{sc} (mA/cm ²)	FF	Best PCE (%)	Average PCE (\pm std dev) ^c (%)
N3	1: 1.2	0.87	8.87	0.60	4.62	4.51 (\pm 0.09)
N4	1: 1.2	0.91	6.69	0.58	3.52	3.41 (\pm 0.08)
N3	1: 2	0.79	7.63	0.47	2.77	2.60 (\pm 0.12)
N4	1: 2	0.87	6.57	0.37	2.10	2.01 (\pm 0.07)
PC ₆₁ BM	1: 1.2 ^b	0.57	8.67	0.63	3.10	2.95 (\pm 0.13)

^a BHJ devices with specified weight ratio. Device structure is ITO/PEDOT: PSS (38 nm)/active layer/Ca (20 nm)/Al (100 nm) with an active layer thickness of \sim 60 nm

^b A standard P3HT: PC₆₁BM device afforded 3.10% efficiency, thereby indicating the reliability of our device fabrication

^c A total of ten devices were made for each combination; cell area = 0.1 cm²

**Fig. S15** IPCE spectra for P3HT: N3 and P3HT: N4.

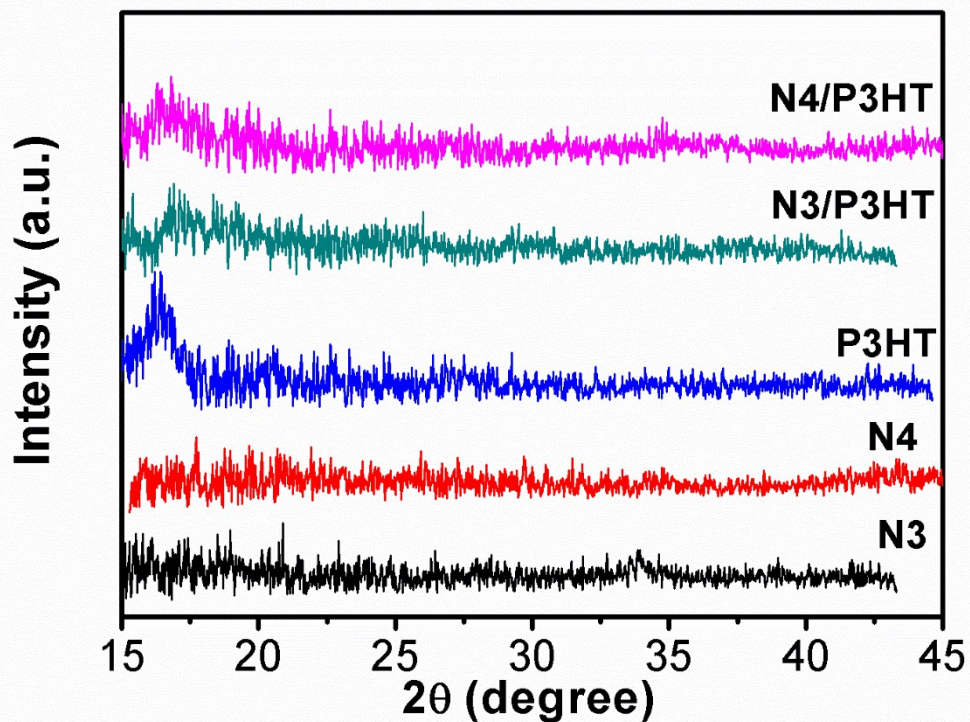


Fig. S16 XRD spectra of neat and blend films of N3 and N4 indicating the surfaces to be amorphous.

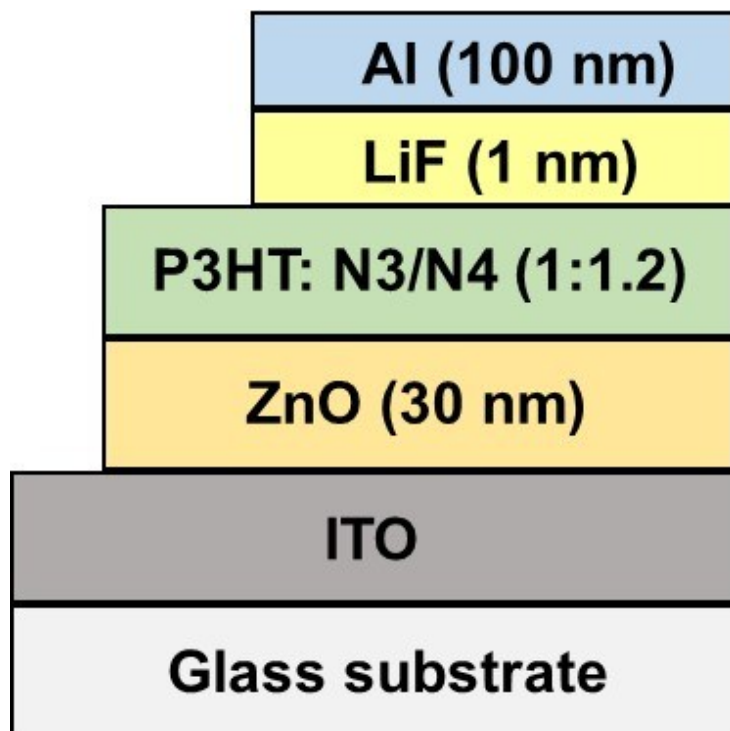


Fig. S17 Device sketch of electron-only devices that was used to study SCLC method.

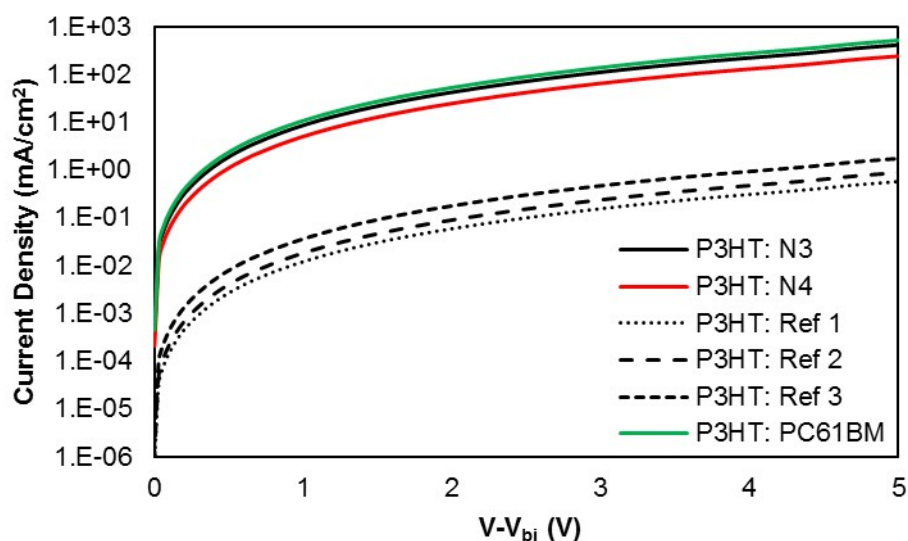


Fig. S18 Current–voltage characteristics of electron only devices which were applied to Mott-Gurney equation to calculate electron mobilities of **N3** and **N4** blends.

[NOTE: In order to compare the electron mobility of the non-fullerene acceptors investigated in the current work with the previously reported in the literature, and to see the influence of terminal accepting functionality on the overall device performance, we concurrently fabricated the electron-only devices using the materials reported in Fig. 1. The literature reported materials [Fig 1; Ref. 1 (Tet. Lett., 2014, 55, 4430) and Ref. 2 (RSC Adv., 2016, 6, 38703)] were employed under the similar experimental set-up (identical to Fig. S17) together with the conventional fullerene acceptor PC₆₁BM. It was found that the electron mobility of **N3** and **N4**, and **N3** in particular, was actually higher than the previously reported examples, almost twofold in magnitude. Considering electron mobility as one of the key factors responsible for better device performance, it is arguable to conclude that the selection of terminal acceptor functionality does play a critical role in the design and development of efficient non-fullerene acceptors stemming from A–A'–A design. The electron mobility of the order of 10⁻³ was observed for PC₆₁BM, a result that corroborates literature finding.]

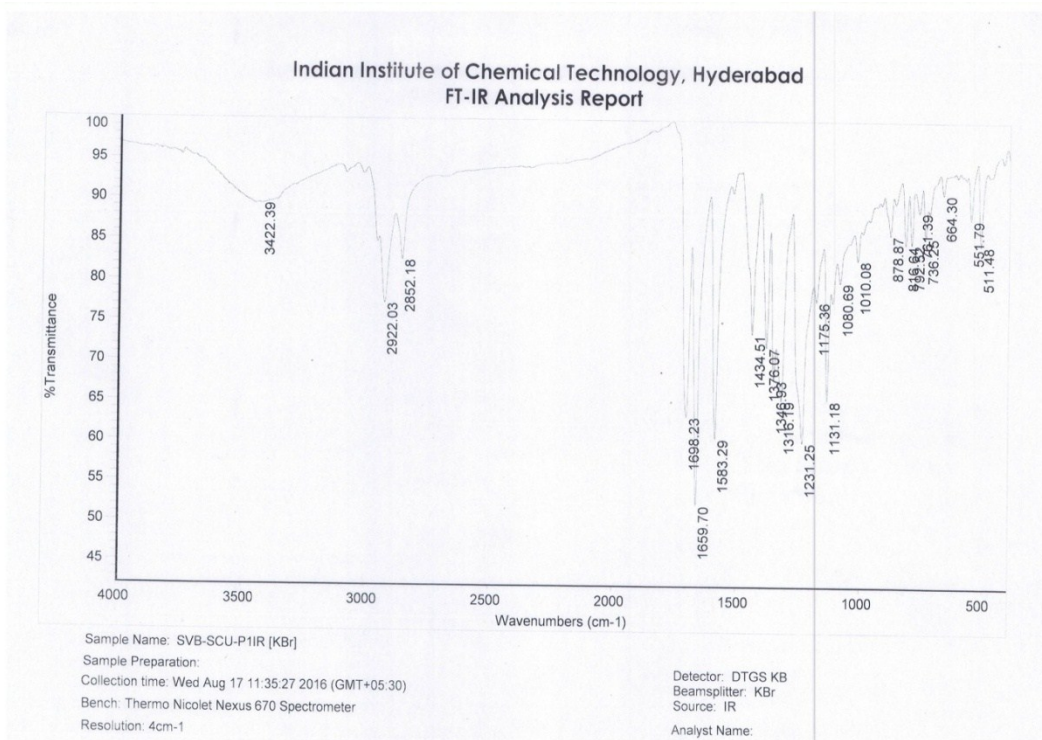


Fig. S21 IR spectrum of N3.

D.SRIVANI, SVB-NER-01

Data: SVB-NER-010001.4A4[c] 4 Oct 2016 11:39 Cal: TOF MIX 04-10-16 RF 4 Oct 2016 11:27
 Shimadzu Biotech Axima Performance 2.9.3.20110624: Mode Reflectron_HiRes, Power: 80, Blanked, P.Ext. @ 2300 (bin 99)
 %Int. 18 mV[sum= 245 mV] Profiles 1-14 Smooth Gauss 5

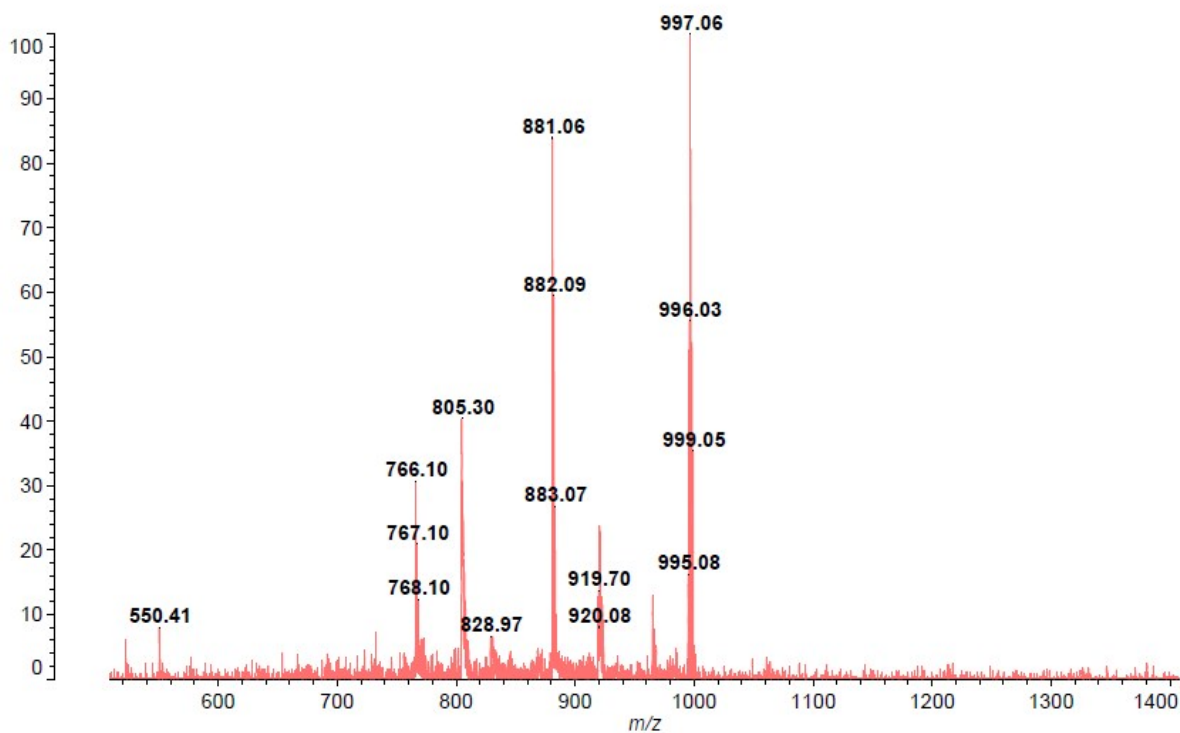


Fig. S22 MALDI-TOF mass spectrum of N3

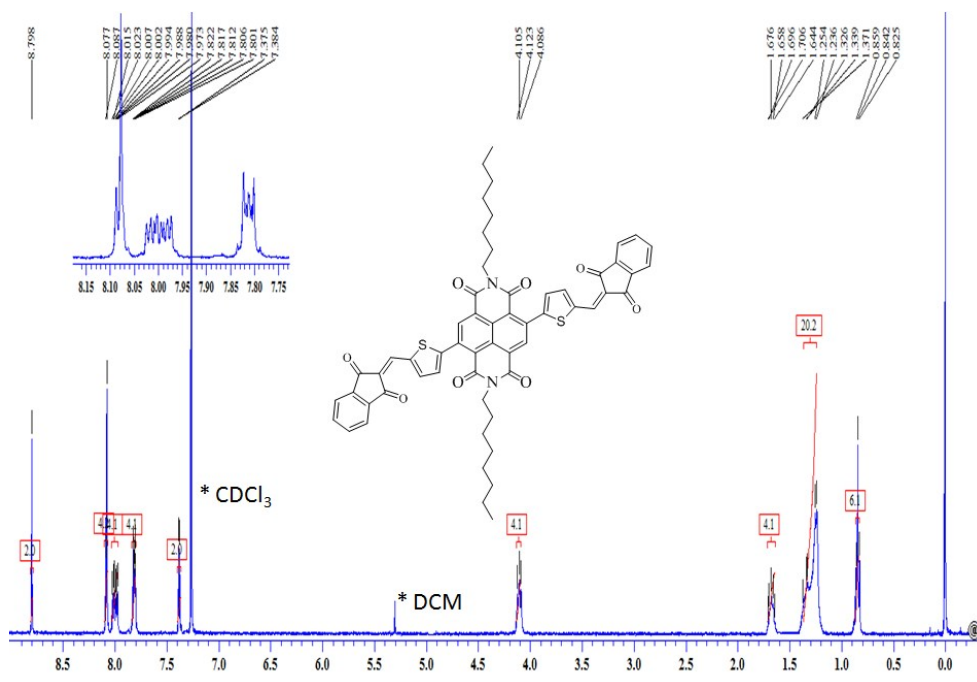


Fig. S23 ¹H NMR spectrum of compound N4 in CDCl₃.

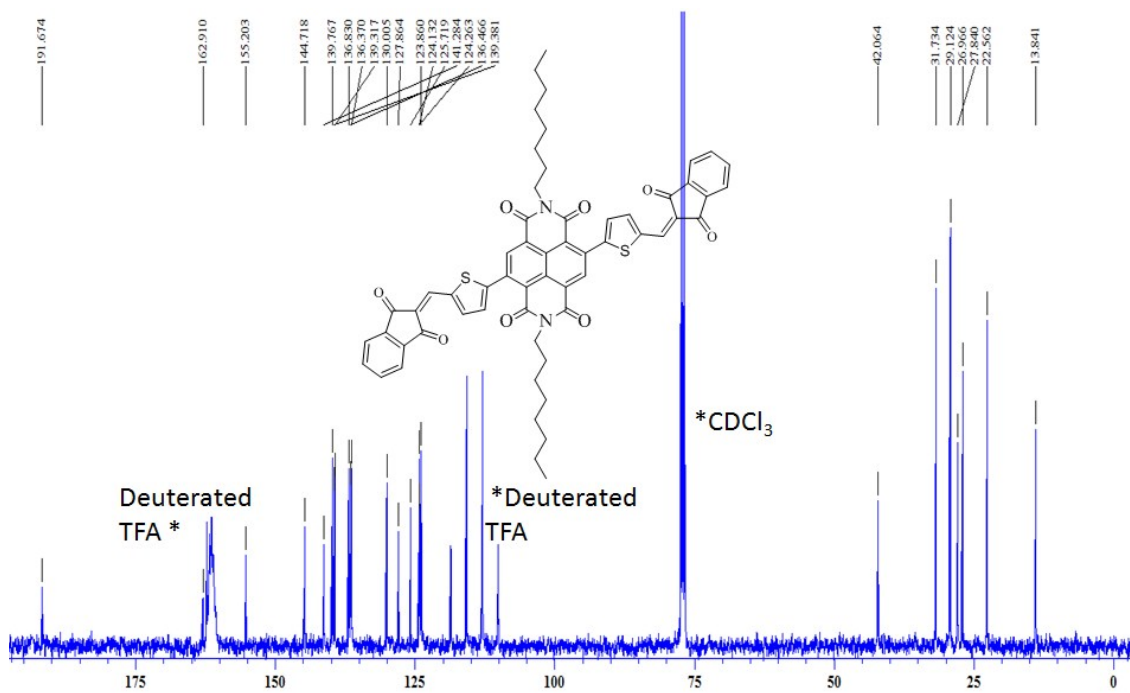


Fig. S24 ¹³C NMR spectrum of compound N4 in CDCl₃, deuterated TFA

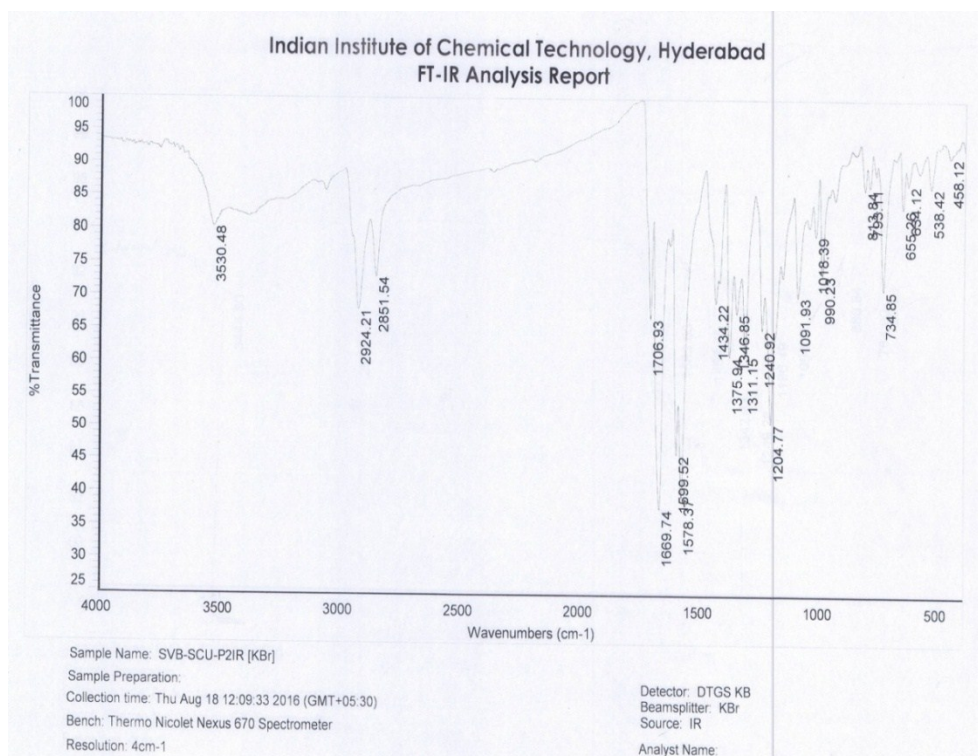


Fig. S25 IR spectrum of N4.

D. SRIVANI, SVB-IDD-01

Data: SVB-IDD-010001.2D1[c] 19 Oct 2016 10:13 Cal: CAL REF-19-10-2016 18 Oct 2016 18:56
 Shimadzu Biotech Axima Performance 2.9.3.20110624: Mode Reflectron_HiRes, Power: 70, Blanked, P.Ext. @ 2300 (bin 99)
 %Int. 61 mV[sum= 3033 mV] Profiles 1-50 Smooth Gauss 5

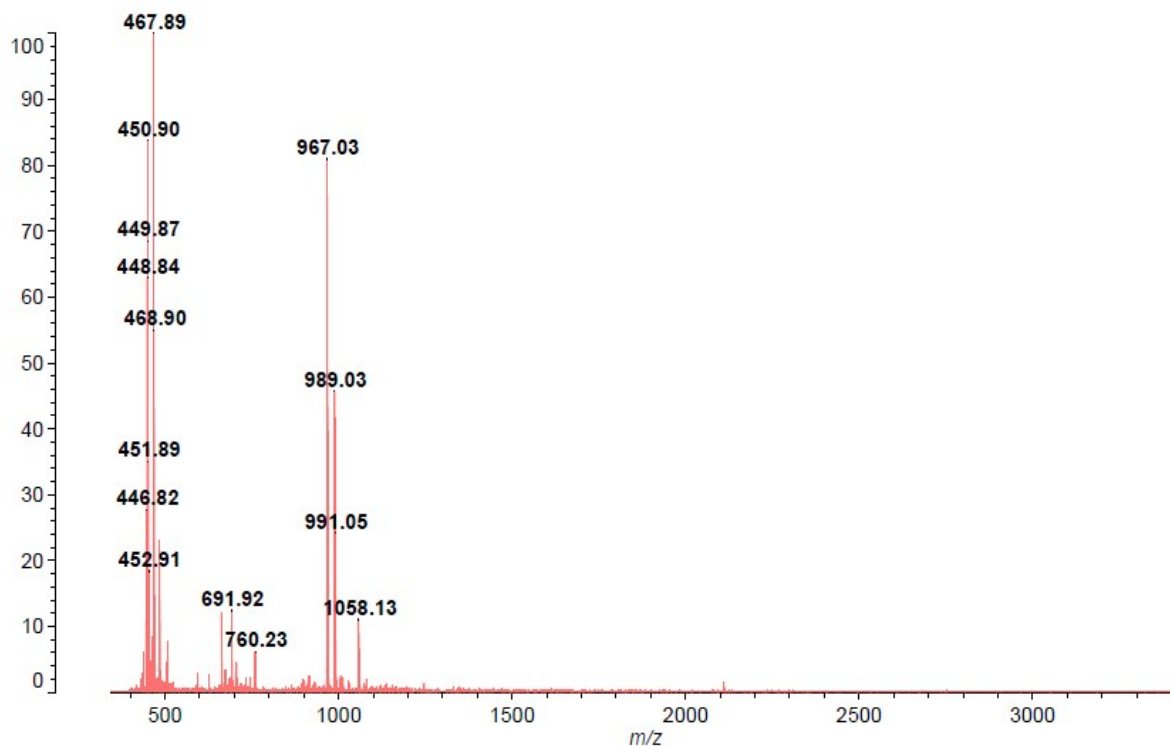


Fig. S26 MALDI-TOF mass spectrum of N4.

References

- S1 D. Srivani, A. Gupta, A. M. Raynor, A. Bilic, J. Li, S. V. Bhosale and S. V. Bhosale, *RSC Adv.*, 2016, **6**, 38703–8.
- S2 A. Gupta, A. Ali, A. Bilic, M. Gao, K. Hegedus, B. Singh et al., *Chem Commun.*, 2012, **48**, 1889–91.
- S3 A. Gupta, V. Armel, W. Xiang, G. Fanchini, S. E. Watkins, D. R. MacFarlane et al., *Tetrahedron*, 2013, **69**, 3584–92.
- S4 Gaussian 09, Revision C.01, M. J. Frisch et al, 2009, Gaussian Inc., Wallingford CT, 2009.
- S5 Avogadro: an open-source molecular builder and visualization tool, Version 1.1.0.; <http://avogadro.openmolecules.net/>
- S6 M.D.Hanwell, D.E. Curtis, D.C. Lonie, T. Vandermeersch, E. Zurek and G. R. Hutchison, “Avogadro: An advanced semantic chemical editor, visualization and analysis platform,” *J.Cheminform.*, 2012, **4**, 1–17.